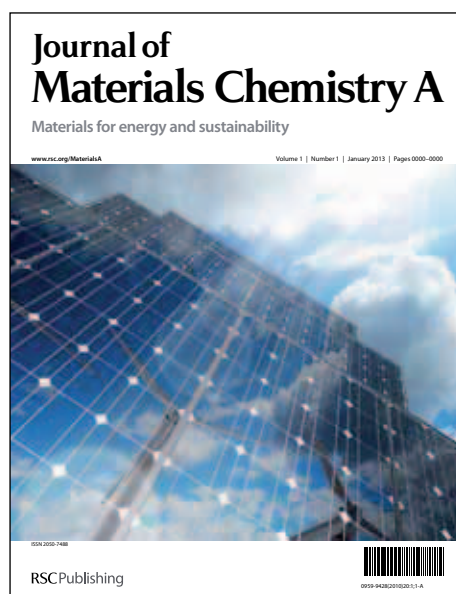


Journal of Materials Chemistry A

Accepted Manuscript



This is an *Accepted Manuscript*, which has been through the RSC Publishing peer review process and has been accepted for publication.

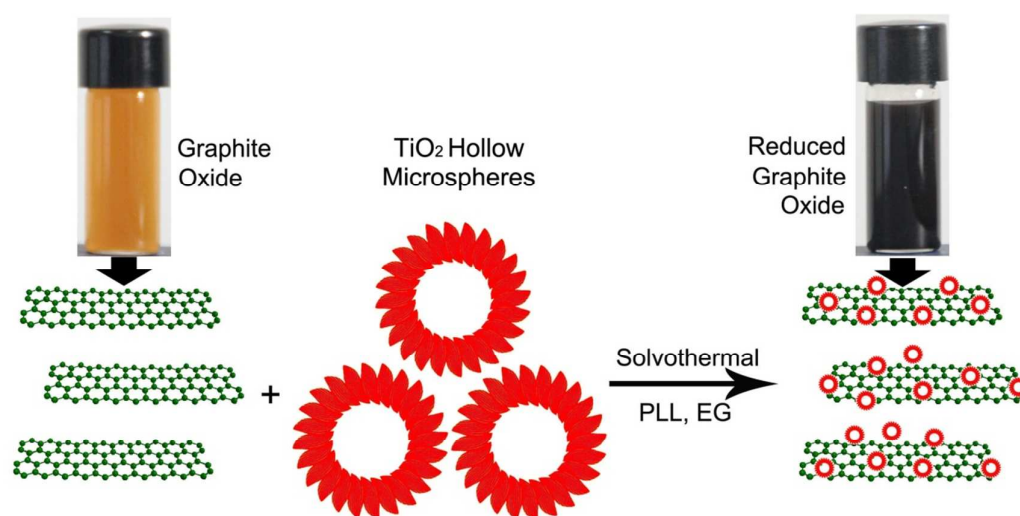
Accepted Manuscripts are published online shortly after acceptance, which is prior to technical editing, formatting and proof reading. This free service from RSC Publishing allows authors to make their results available to the community, in citable form, before publication of the edited article. This *Accepted Manuscript* will be replaced by the edited and formatted *Advance Article* as soon as this is available.

To cite this manuscript please use its permanent Digital Object Identifier (DOI®), which is identical for all formats of publication.

More information about *Accepted Manuscripts* can be found in the [Information for Authors](#).

Please note that technical editing may introduce minor changes to the text and/or graphics contained in the manuscript submitted by the author(s) which may alter content, and that the standard [Terms & Conditions](#) and the [ethical guidelines](#) that apply to the journal are still applicable. In no event shall the RSC be held responsible for any errors or omissions in these *Accepted Manuscript* manuscripts or any consequences arising from the use of any information contained in them.

3D structured rGO/TiO₂ composite was firstly synthesized by a simple solvothermal reaction using Poly (L-Lysine) (PLL) and ethylene glycol (EG) as coupling agent. The composite shows markedly enhanced photocatalytic activity compared to synthesized simply mixture of TiO₂ and GO, original TiO₂, and the commercial P25 for the photocatalytic degradation of MB.



Cite this: DOI: 10.1039/c0xx00000x

www.rsc.org/xxxxxx

ARTICLE TYPE

A novel 3D structured reduced graphene oxide/TiO₂ composite: synthesis and photocatalytic performance

Wang Yan,^a Fei He,^a Shili Gai,^a Peng Gao,^{*a} Yujin Chen^{*b} and Piaoping Yang^{*a}

Received (in XXX, XXX) Xth XXXXXXXXX 20XX, Accepted Xth XXXXXXXXX 20XX

DOI: 10.1039/b000000x

In this study, TiO₂ hollow microspheres with the highest photocatalytic activity were prepared by simply optimizing the ratio of the as-used templates (poly (4-styrenesulfonate) (PSS) and triblock copolymer P123). In particular, a novel three-dimensional (3D) reduced graphene oxide/TiO₂ (rGO/TiO₂) hybrid composite was for the first time prepared by wrapping TiO₂ hollow microspheres with rGO sheets *via* a facile solvothermal route using poly (L-Lysine) (PLL) and ethylene glycol (EG) as coupling agent. The structural, morphological and photocatalytic properties of as-synthesized products were well examined. It is found that rGO/TiO₂ hybrid composite exhibit markedly enhanced photocatalytic performance in comparison with pure TiO₂ hollow microspheres and the simply mixture of rGO and TiO₂ spheres. The rational design, interesting structure and the ideal photocatalytic performance of this graphene-based composite show highly promising in diverse fields.

1 Introduction

Recently, intense research on effective semiconductor photocatalyst has attracted a lot of interest owing to their fundamental and technological applications to environmental purification.¹⁻⁹ As one of the most popular photocatalysts, titanium dioxide has attracted significant attention due to its photochemical stability, long-term stability against photocorrosion and chemical corrosion, relative nontoxicity, low-cost, and thus can be applied in diverse fields such as paints, dye-sensitized solar cells, lithium ion batteries, microbial fuel cells, sensor, photocatalysis, electrocatalysis and drug delivery system.¹⁰⁻¹⁹

Anatase and rutile are the two main crystalline phases of TiO₂ which are commonly used in photocatalysis.^{20,21} Different structures of the two phases exhibit different physical properties, leading to diverse applications. It is widely accepted that photocatalytic reactions mainly take place on the surfaces of the photocatalysts. The efficiency of titania highly depends on their size, composition, crystal phase, crystallinity, specific surface area and morphology. Thus, controlling the morphology and structure of titania is an important issue in terms of optimizing their properties.²²⁻²⁸ Up to now, remarkable progress has been made in the preparation of TiO₂ nanocrystals, tubes, rods, and nanowires.⁵ Many methodologies have been developed for the fabrication of titania materials with diverse phases, morphologies and structures. Li *et al.* prepared TiO₂ annealed at different temperatures, and the surface phases of TiO₂ were studied.²⁷ Fu *et al.* synthesized stable porous TiO₂ photocatalysts with high photocatalytic activity *via* a hydrothermal process, followed by a post treatment in the presence of ethylenediamine.²⁹ These processes usually concerning an annealing temperature have been

regarded as novel method for the fabrication of titanium dioxide. However, their disadvantages, including long reaction time, high annealing temperature, tedious synthetic procedures greatly hinder their applications. In particular, high annealing temperature often causes particle agglomeration which will result in surface area decline and undesired phase transformation, leading to the obvious decrease of photocatalytic activity. Therefore, it will be highly promising to establish a mild, facile, and economic strategy for preparing high quality TiO₂ with controlled phase/morphology, which can overcome above mentioned shortcomings.³⁰ Moreover, solvothermal process has been proved to be one of the most convenient, effective, and facile approaches for the preparation of homogeneous metal oxides at relatively lower temperature and shorter reaction time which avoided the annealing process. Furthermore, 3D TiO₂ with tunable structures and phases by simply altering the amounts of the surfactants *via* a solvothermal process has never been reported.

TiO₂ with different structures have been extensively employed as catalysts for photocatalytic reaction. However, there is still a great challenge to further promote the photocatalytic activity for the growing concerns about air/water pollution. So far, there have been several investigations on improvement of photocatalytic efficiency of TiO₂, such as depositing noble metals and doping metal or nonmetal ions.³¹⁻³⁴ These composites indeed showed photocatalytic enhancement to certain extent. Among them, the combination of TiO₂ with the graphene-based derivatives such as graphene oxide (GO), reduced graphene oxide (rGO) materials have attracted much attention because of the excellent mechanical property, large surface area, and flexible structures.

As a two-dimensional (2D) sheet with fully delocalized sp²-bonded carbon atoms, graphene sheets has advantages over other

materials including high surface area with electronic conductivity, mechanical robustness, stable in electrochemical environments, thermal conductivity, electrical conductivity and can be chemically functionalized.^{35–43} Due to its attractive chemical structure, there is interest in using single layer graphene and other graphene derivatives for a variety of applications in catalytic activity, supercapacitors, lithium-ion batteries, energy storage and conversion.^{44–54} Zhang *et al.* reported the fabrication of graphene encapsulated hollow TiO₂ nanospheres by a hard template method but it involves preparation of SiO₂, calcination process and final etching of the template.⁵⁵ However, uniform mixed phase TiO₂ hollow microspheres prepared by one spot route and arranged on reduced graphene have never been reported so far. In our 3D rGO/TiO₂ composite, the TiO₂ spheres are arranged on the reduced graphene sheets which can not only improve the surface area of the composite but prevent agglomeration or the irreversibly restack to form graphite. The crinkled texture and the 3D structure of rGO ensure that sufficient catalytic reaction to take place easily. As mentioned above, the rGO sheets can extend out of the composite without agglomeration which can provide better access for the solution into the entire structure. Therefore, it is reasonable that the rGO/TiO₂ composite has a higher photocatalytic activity than other samples in our work. As a result, from the perspective of application, developing a new family of graphene-based materials with diverse well-defined novel morphologies *via* rapid, simple, and low cost method should be highly promising and attractive.

In our contribution, we proposed a facile and universal approach for producing of different morphologies/phases TiO₂ structures with 3D hollow structure firstly. P123 and PSS were used in the solvothermal process, the morphologies and phases of the samples can be controlled by simply adjusting the amount and concentration of the surfactant. Then, graphene-based TiO₂ hybrid composite was prepared with the aid of PLL and EG by a solvothermal rout. GO is then reduced to graphene *via* the thermal treatment and TiO₂ particles were arranged on the rGO. Notably, PLL and EG were used as coupling agent during the process and they are the only reagents involving, which reduces energy consumption and prevents the possible contamination of the toxic chemicals. PLL is commonly known as a unique molecule capable of mimicking the adhesive proteins which is present in various animals and it can autopolymerize to form a coating on almost all material surfaces. GO nanosheets and the TiO₂ spheres were coated with PLL and EG through electrostatic adsorption between the negative charges on GO and the positive charges of PLL. As a result, TiO₂ particles were arranged on the rGO surface. Moreover, the photocatalytic properties of as-prepared hollow TiO₂ microspheres, simple mixture of GO and TiO₂, rGO/TiO₂ composite were investigated in detail.

2 Experimental section

Reagents and materials

All materials including titanium tetraisopropanlate, triblock copolymer Pluronic P123 and sodium poly (4-styrenesulfonate) (PSS) with average molecular weights of 70,000, poly (L-Lysine) (PLL), absolute ethanol, HCl, NaOH, ethanolethylene glycol

(EG) were purchased from Sinopharm Chemical Reagent Co., Ltd and used as received without further purification.

Synthesis procedure

Graphite oxide (GO) was prepared from natural graphite according to the modified Hummers method. GO solution was prepared by long time sonication of GO in deionized water.

In a typical procedure for the synthesis of TiO₂ with W_R of 20.8%, 0.08 g of P123 and 7 mL of ethanol were added to an aqueous solution containing PSS (20 mL, 0.5 g/L) and stirred until P123 was dissolved. Then 0.5 mL titanium tetraisopropanlate was added to the mixture. After that, 3 mL HCl was added. After additional agitation for 5 min, the resultant solution was transferred to a 50 mL autoclave and maintained at 180 °C for 12 h. Finally, the autoclave was cooled to room temperature naturally. The precipitates were separated by centrifugation, followed by washing with deionized water and ethanol several times. The final product was dried at 60 °C in air overnight. TiO₂ architectures with different morphologies and phase were prepared by a similar process only by changing the P123 amount and the PSS concentration in the initial solution. The weight fraction of anatase phase to rutile phase was calculated by $W_R = 1/(1+0.884(A_{ana}/A_{rut}))$, where A_{ana} and A_{rut} denote the X-ray integrated intensity values of anatase (101) and rutile (110) diffraction peaks, respectively. The detailed added concentration of P123 and PSS and the corresponding calculated W_R are list in Table 1.

The 3D rGO/TiO₂ composite were prepared by a solvothermal process. Typically, 20 mL GO solution (1 mg/mL), 200 mg PLL and 20 mL EG were mixed together and stirred for 20 min. After that, 0.07 g 3D hollow TiO₂ microspheres were added into above solution with continuous stirring for 15 min at room temperature. The pH value of the mixed solution was adjusted to 11 by NaOH solution. After additional stirring for 8 h, the suspension was then transferred into a 100 mL autoclave and heated at 180 °C for 12 h. After naturally cooled down to room temperature, the precipitates were separated by centrifugation and then washed several times with deionized water and ethanol. For comparison, the simply mixture of rGO and TiO₂ was prepared by sonicating 0.07 g of 3D TiO₂ hollow microspheres ($W_R = 20.8\%$) with 20 mg of GO in 20 mL deionized water for 1 h. After that, the suspension was then collected by centrifugation.

Characterization

X-ray diffraction (XRD) measurement was conducted on a Rigaku D/max-TTR-III diffractometer using Cu K α radiation ($\lambda = 0.15405$ nm). The morphologies of the samples were inspected on a scanning electron microscope (SEM, JSM-6480A, Japan Electronics). Transmission electron microscopy (TEM) and high-resolution transmission electron microscopy (HRTEM) micrographs were performed on a FEI Tecnai G² S-Twin transmission electron microscope with a field emission gun operating at 200 kV. Raman spectra were recorded on a Renishaw RM2000 Raman spectrometer with 457.9 nm wavelength incident laser light. The X-ray photoelectron spectra (XPS) were performed on a VG ESCALAB MK II electron energy spectrometer using Mg KR (1253.6 eV) as the X-ray excitation source. The N₂ adsorption/desorption isotherms were

Table 1 Sample names and corresponding experimental conditions

Sample	P123 (g)	PSS (g/L)	W_R (100%)
A	0.08	0	0
B	0.08	0.05	20.8
C	0.08	0.075	50.4
D	0.08	0.1	74.1
E	0	0.125	100

conducted with a liquid nitrogen temperature ($-196\text{ }^\circ\text{C}$) using a Micromeritics ASAP 2010 instrument. The specific surface area was calculated by the Brunauer-Emmett-Teller (BET) method. All of the measurements were performed at room temperature.

Photocatalytic experiments

In a typical process, aqueous solution of the MB dyes (20 mg/L, 200 mL) and the photocatalysts (TiO_2 with different W_R , rGO/ TiO_2 composite, simply mixture of TiO_2 ($W_R = 20.8\%$) and GO, and P25) were placed in a cylindrical quartz vessel, A 500 W high-pressure mercury lamp was used as a light source which was placed at about 10 cm from the reactor above. After the mixture was premixed for 60 min, the light was turned on to initiate the reaction. The concentrations of MB solutions before and after UV irradiation were determined by a UV-visible spectrophotometer (UV-2550, Shimadzu) from the absorbance at 664 nm.

3 Results and discussion

Phase, structure and photocatalytic activity of TiO_2

Fig. 1 shows the XRD patterns of TiO_2 prepared with different additives (PSS/P123), and the corresponding SEM images of the samples are given in Fig. 2. It can be seen that the size and morphology of the samples prepared with different additive ratio are much different. In Fig. 1A for the sample prepared with 0.08 g P123 and absence of PSS ($W_R = 0$), the diffraction peaks can be directly indexed to anatase phase (JCPDS No. 21-1272). The corresponding SEM image (Fig. 2A) and TEM image (inset) shows that the irregular shaped and aggregated particles are produced. When the PSS concentration is increased to 0.05 g/L and P123 is fixed at 0.08 g ($W_R = 20.8\%$), the rutile phase begins to appear and the anatase phase is still predominant (Fig. 1B),

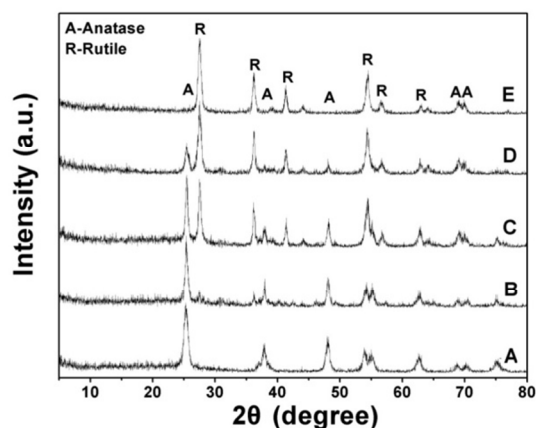


Fig. 1 XRD patterns of TiO_2 prepared with different additive: 0.08 g P123 (A), 0.05 g/L PSS and 0.08 g P123 (B), 0.075 g/L PSS and 0.08 g P123 (C), 0.1 g/L PSS and 0.08 g P123 (D), 0.125 g/L PSS (E). The respective W_R is 0%, 20.8%, 50.4%, 74.1%, and 100%.

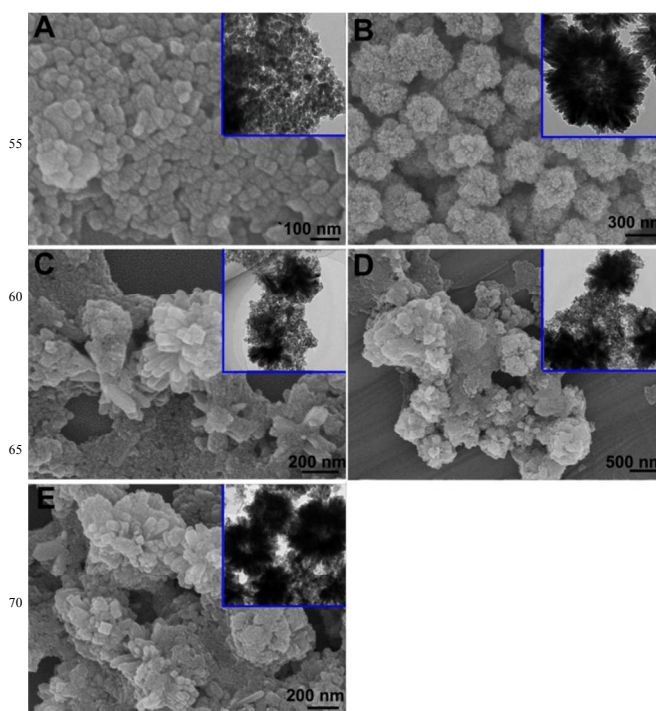


Fig. 2 Low- and high-magnification SEM images of TiO_2 prepared with different additive: 0.08 g P123 (A), 0.05 g/L PSS and 0.08 g P123 (B), 0.075 g/L PSS and 0.08 g P123 (C), 0.1 g/L PSS and 0.08 g P123 (D), 0.125 g/L PSS (E). Insets are their corresponding TEM images.

indicating the sample partially transforms from anatase phase to rutile phase with the help of PSS. It is interesting that as-prepared sample consists of well-defined quasi-flower-like 3D structured spheres and with relatively narrow size range. In particular, hollow structure can be confirmed from the pale center and dark outside edge (inset in Fig. 2B), which should be derived from the used surfactant. As the PSS concentration is changed to 0.075 g/L and P123 is fixed at 0.08 g ($W_R = 50.4\%$), the rutile phase grows obviously (Fig. 1C). When the PSS concentration is raised to 0.1 g/L and P123 is fixed at 0.08 g ($W_R = 74.1\%$), a considerable amount of anatase phase transforms into rutile phase, which become predominant. Irregular sphere-like aggregates with some nanoparticles are obtained (Fig. 2D). As for the sample prepared with 0.05 g/L PSS and absence of P123, the diffraction peaks can be well indexed to rutile-phased TiO_2 (JCPDS No. 21-1276), indicating the complete transformation to rutile phase. Irregular aggregates composed of hollow spheres are obtained (Fig. 2E and inset). It can be concluded from the above results that higher PSS concentration would inhibit the formation of anatase-phased TiO_2 , meanwhile promoting the formation of the rutile-phased TiO_2 . These results clearly suggest that PSS plays an important role in the phase and structure of the final products, which has been proved in our previous work and other related reports.⁵⁶⁻⁵⁸

To investigate the photocatalytic performance of the TiO_2 with different architectures, systematic photocatalytic tests were carried out by using MB as a model dye due to its stable photochemical property. The photocatalytic degradation rates of MB on the different TiO_2 samples are displayed in the Fig. 3. It is obvious that the sample prepared with 0.08 g P123 and 0.5 g/L PSS displays the highest activity among the as-prepared five TiO_2 samples. Based on the above XRD, SEM and TEM results, it can

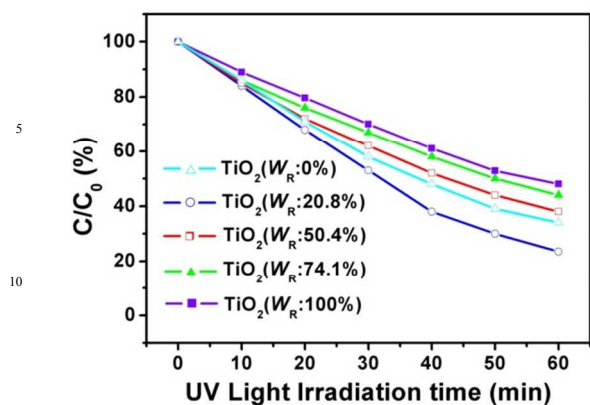


Fig. 3 Photodegradation of MB aqueous solution for TiO₂ ($W_R = 0\%$), TiO₂ ($W_R = 20.8\%$), TiO₂ ($W_R = 50.4\%$), TiO₂ ($W_R = 74.1\%$), TiO₂ ($W_R = 100\%$).

be concluded that the high activity of the TiO₂ ($W_R = 20.8\%$) sample should be attributed to the high dispersity, well defined 3D hollow structure and especially the mixed phased of 79.2% anatase and 20.8% rutile.

To understand the growth mechanism of the hollow TiO₂ architecture ($W_R = 20.8\%$), systematic time-dependent experiments were carried out at 180 °C. The TEM images of the product obtained after 20 min, 3 h, 6 h and 12 h in the solvothermal process illustrate the morphology evolution of the hollow TiO₂ architectures (Fig. 4). In Fig. 4A, the sample collected after solvothermal treatment for 20 min leads to the formation of amorphous nanoparticles which is unstable and is susceptible to attach to each other with the help of the surfactants. The sulfonic groups in the molecular chain have a strong tendency to attract positively charged ions or to be attached on positively charged surfaces. The interaction between PSS and P123 leads to their aggregation and hydrophilic-hydrophobic interactions associated with the pendent chains of the adsorbed copolymers, cooperative with the anisotropy of TiO₂ primary nanoparticles, making those polymer TiO₂ primary nanoparticles spontaneously assemble into 3D spherical structures. As the reaction time is increased to 3 h, some sphere aggregation with a

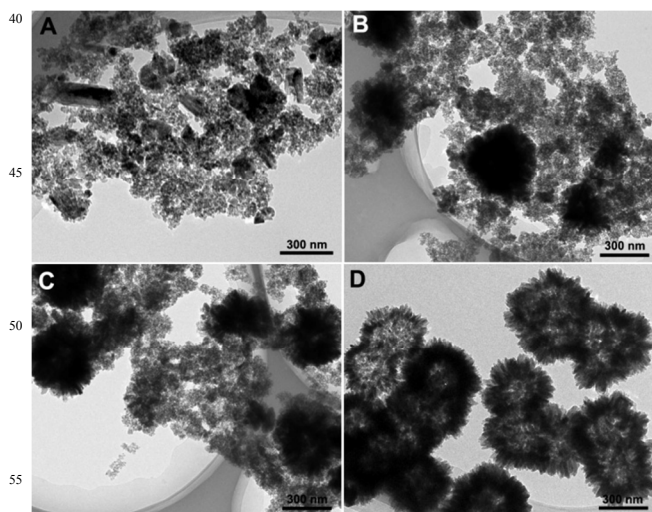
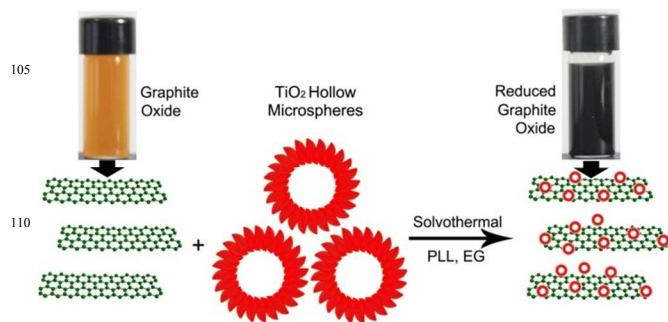


Fig. 4 TEM images of TiO₂ ($W_R = 20.8\%$) prepared at 180 °C for reaction time of (A) 20 min, (B) 3 h, (C) 6 h and (D) 12 h.

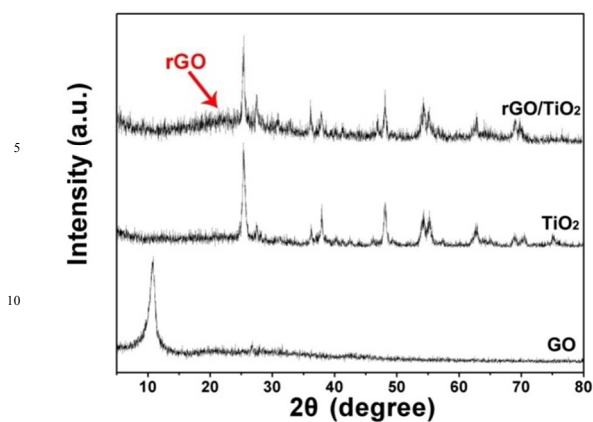
solid interior are obtained (Fig. 4B). With further reaction, nanoparticles attach on the surface of the sphere aggregation and the underdeveloped structures grow. Further prolonging the reaction time to 6 h, the microstructures grown in all directions and the hollow morphology is observed (Fig. 4C). Furthermore, as the reaction proceeds to 12 h, the underdeveloped hollow architectures continue to grow by combining the remaining primary nanoparticles and the shell of the hollow spheres becomes denser with more nanoparticles. As a result, fully developed TiO₂ hollow spheres formed, the interior structure is clearly shown in Fig. 4D, which is due to a dissolution-renucleation process during the reaction and it is proposed on the basis of Ostwald ripening. Large crystals grow at the expense of small ones by the diffusion of ions, atoms or molecules within an ensemble of crystalline materials.

Phase, structure, and photocatalytic activity of rGO/TiO₂

As discussed above, we found that the rational control of the weight ratios of rutile phase in the mixed phase is important to the photocatalytic performance of the materials. TiO₂ hollow spheres prepared with 0.08 g P123 and 0.05 g/L PSS ($W_R = 20.8\%$) shows the superior photocatalytic property to others. However, there is still a great challenge to further improve the photocatalytic activity. Thus, we proposed a facile and universal route to prepare 3D TiO₂ arranged on reduced graphene oxide hybrid composite (rGO/TiO₂) with the aid of PLL and EG at 180 °C for 12 h by the solvothermal process. GO was reduced to rGO after the thermal treatment and hollow TiO₂ microspheres were arranged on the rGO sheets. This approach is schematically illustrated in Scheme 1. To identify the phase and the structure of TiO₂ and rGO/TiO₂ composite, XRD patterns of pure GO, TiO₂, and rGO/TiO₂ were examined, which are shown in Fig. 5. According to the result of the XRD analysis, a characteristic peak of GO appeared at $2\theta = 9.9^\circ$ which matched earlier results and the results confirmed that GO was successfully synthesized from graphite by the modified Hummers' method. And it shows the characteristic peaks of the mixed anatase and rutile phases of TiO₂. Compared with pure TiO₂, the major diffractions of rGO/TiO₂ composite are almost unchanged, indicating that mixed phase can be well maintained in the composite. The wide angle XRD data of as-made composite showed a broad peak at $2\theta = 25^\circ$ which attributed to rGO indicating the thermal reduced graphene (002) plane after the solvothermal process. Moreover, for the rGO/TiO₂ composite, the disappearance of the GO peak at $2\theta = 9.9^\circ$ also confirms the reduction of GO to rGO in the composite.



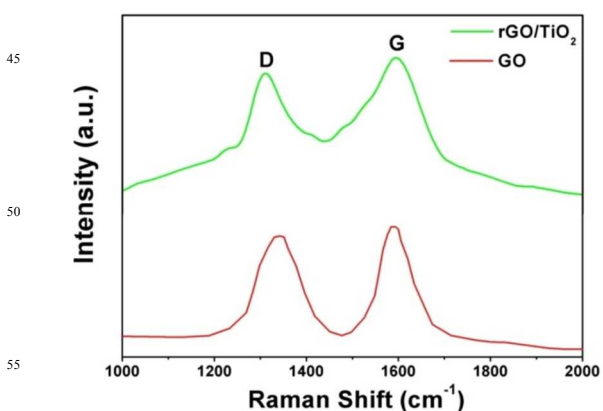
Scheme 1 Schematic illustration for the formation process of rGO/TiO₂ composite.



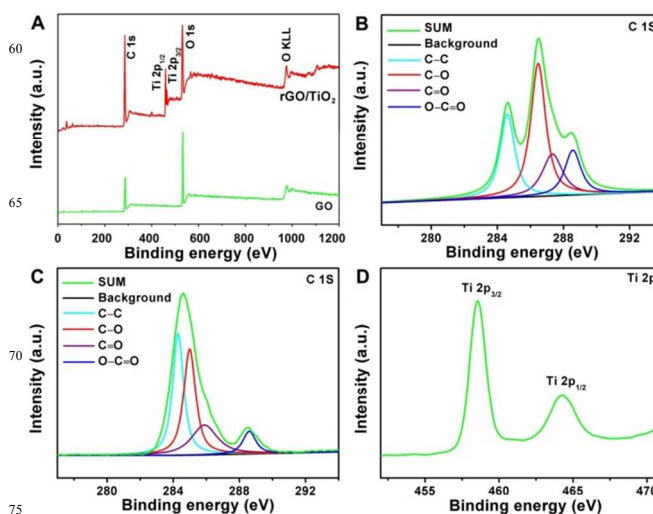
15 **Fig. 5** XRD patterns of GO, TiO₂, and rGO/TiO₂ composite.

Fig. 6 shows the Raman spectra of pristine graphene sheets and the rGO/TiO₂ composite. It is shown that both of the curves show two bands at 1590 cm⁻¹ (G band), and 1350 cm⁻¹ (D band) which confirm the presence of carbon materials. The G bands are responsible for E_{2g} phonon corresponding to sp² atoms, while the D band is associated with the defects, curved sheets and dangling bonds in the carbon structures.⁵⁹ Peak intensity ratio of the D and G band (*I_D/I_G*) is inversely proportional to the extent of sp² domain and can be used to estimate the disorder degree and average size of the sp² domains of the graphite materials.⁶⁰ Compared to that of GO, the decreased *I_D/I_G* ratio (0.857 for rGO/TiO₂ and 0.997 for GO) of rGO/TiO₂ indicates a typical graphene structure obtained by the thermal reduction.

The surface chemical information of the products was examined by XPS analysis. Fig. 7 gives the survey and elements XPS spectra of GO and rGO/TiO₂, respectively. As shown in Fig. 7A, pure GO nanosheet exhibits individual peak at 284.5 eV in the XPS spectra. The survey spectrum of the rGO/TiO₂ composite mainly shows carbon, oxygen and titanium species. In Fig. 7B for C1s spectrum of GO, the deconvolution of C1s spectrum of GO indicates the presence of four types of carbon bonds: C–C (284.5 eV), C–O (286.2 eV), C=O (287.2 eV), and O–C=O (288.3 eV).⁶¹ Compared to pure GO, the peaks of rGO/TiO₂ related to the oxidized carbon, especially the peak of C–O decrease greatly, indicating that GO has been well deoxygenated to form graphene (Fig. 7C). And the peaks related with C–C or C=C (284.5 eV) become predominant for the reduced GO. The increased



45 **Fig. 6** Raman spectra of the pristine GO sheets and rGO/TiO₂ composite.



65 **Fig. 7** XPS spectra of the pure GO sheets and as-prepared rGO/TiO₂ composite. XPS survey spectra (A), C1s spectrum of GO (B), C 1s spectrum of rGO/TiO₂ composite (C) and Ti 2p spectrum of the rGO/TiO₂ composite (D).

restoration of the sp² hybridised carbon atoms (C–C) for rGO/TiO₂ composite indicates higher extent of graphite oxidation during synthesis of this composite, indicating that GO has been well deoxygenated to form graphene. Additionally, two major peaks of Ti 2p centered at 459.2 associated with the Ti 2p_{3/2} and Ti 2p_{1/2} confirm the presence of TiO₂ (Fig. 7D). The XPS results are well consistent with above XRD and Raman analysis.

The morphologies and structure of the as-synthesized TiO₂ and rGO/TiO₂ were further investigated. The low-magnification SEM image (Fig. 8A) reveals that the hollow spheres are quite uniform with high morphological yield and have a relatively narrow size distribution. The size of the hollow spheres ranges from 200 to 400 nm with an average diameter of about 300 nm. The magnified SEM image of TiO₂ (Fig. 8B) indicates that the hierarchical architecture has hollow structured interiors which is obvious in Fig. 8B labeled by the red circle. TEM image of TiO₂ (Fig. 8C) proves that the as-synthesized TiO₂ has a hierarchical 3D structure and the size and shape are similar to those in the SEM images. The magnified TEM image in Fig. 8D reveals that the 3D structures have hollow interiors manifested by the obvious contrast between the darker edge and lighter pale center. Moreover, close observation reveals that these hollow spheres are composed of numerous nanorods/nanosheets standing along the radial direction of the spheres and seemed to be quite flexible. The interesting structure should be beneficial to the photocatalytic activity of the product. Fig. 8E displays the TEM image of GO. The characteristics of 2D rGO with a little curved and crinkled texture are observed, which is common at the edge of the typical GO. In Fig. 8F for rGO/TiO₂ obtained *via* the solvothermal process, graphene sheets with crinkled textures are clearly found on the composite, and most of TiO₂ spheres are arranged on the reduced graphite oxide due to the flexible and rough properties of rGO sheets. Moreover, as shown in the TEM images (Fig. 8G and H), it is apparent that TiO₂ hollow spheres with good dispersibility are well encapsulated by the rGO sheets. Notably, the encapsulation the TiO₂ hollow spheres by the rGO sheets should be able to increase the surface area and avoid the

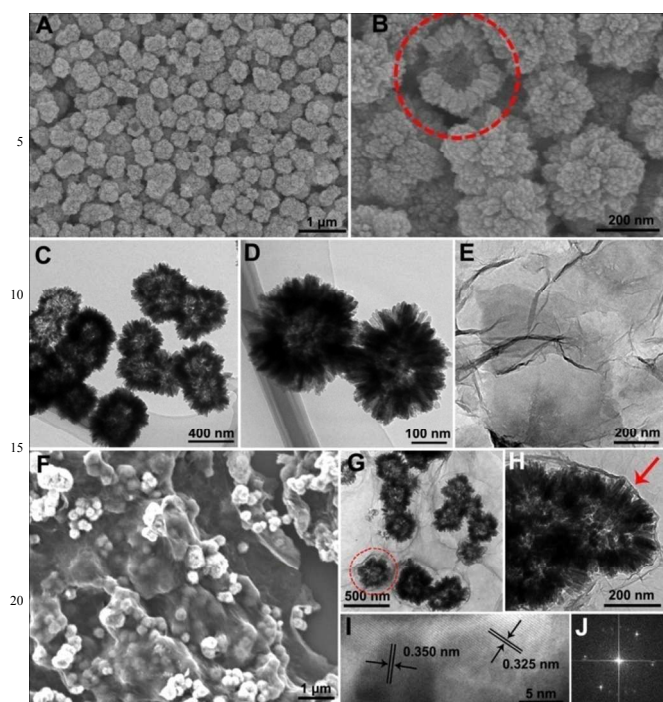


Fig. 8 Low- (A), high-magnification (B) SEM images and TEM image of TiO_2 (C, D); TEM image of GO (E); SEM image (F), TEM images (G, H), HRTEM image (I), and the corresponding FFT pattern of rGO/ TiO_2 composite (J). Inset in panel (A) is the size distribution of the as-synthesized sample.

agglomeration of the particles. For comparison, the morphology between the rGO/ TiO_2 composite and simple mixture of GO and TiO_2 spheres are shown in Fig. S1. Different from the composite, the separated structure of rGO and TiO_2 are observed in the simple mixture of GO and TiO_2 spheres sample. The inferior contact between the TiO_2 spheres and rGO can be ascribed to the absence of PLL and EG during the solvothermal process. In the HRTEM image (Fig. 8I), the measured interplanar distance of 0.350 nm corresponds to the (101) plane spacing of anatase TiO_2 , and the interplanar distance of 0.325 nm matches well with the (110) plane spacing of rutile TiO_2 . This is also supported by the corresponding fast Fourier transform (FFT) pattern of the sample (Fig. 8J).

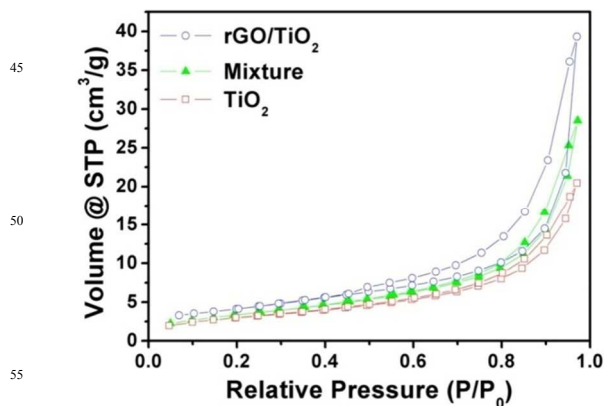


Fig. 9 N_2 adsorption/desorption isotherms of TiO_2 ($W_R = 20.8\%$), simply mixture of TiO_2 ($W_R = 20.8\%$) and GO, and rGO/ TiO_2 composite.

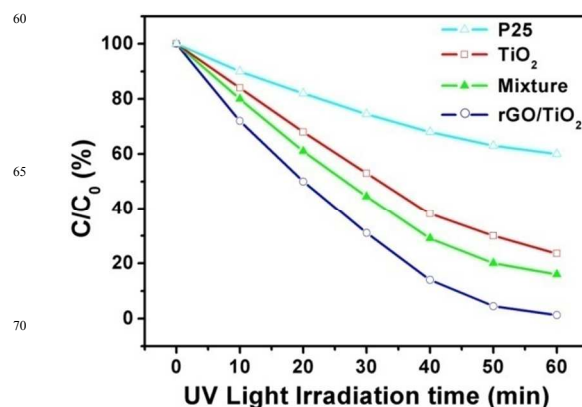


Fig. 10 Photodegradation of MB aqueous solution for TiO_2 ($W_R = 20.8\%$), rGO/ TiO_2 composite, simply mixture of TiO_2 ($W_R = 20.8\%$) and GO, and P25.

Fig. 9 gives the N_2 adsorption/desorption isotherms of TiO_2 ($W_R = 20.8\%$), simply mixture of GO and TiO_2 spheres, and rGO/ TiO_2 composite. As shown, all the samples exhibit typical IV-typed isotherms, indicating the mesoporous nature of all the samples. The BET surface area and total pore volume are calculated to be 124.1, 153.1, 180.8 m^2/g and 0.445, 0.609, 0.735 cm^3/g for TiO_2 ($W_R = 20.8\%$), simply mixture of GO and TiO_2 spheres and rGO/ TiO_2 composite, respectively.

To study the photocatalytic activity, systematic photocatalytic tests were carried out on TiO_2 ($W_R = 20.8\%$), rGO/ TiO_2 composites using MB as the model dye. For comparison, simple mixture of GO and TiO_2 spheres and the commercial Degussa P25 were also tested. Fig. 10 presents the photocatalytic activity of four catalysts. As expected, all the products exhibit degradation property to MB. TiO_2 ($W_R = 20.8\%$) displays higher degradation ratio of MB than that of Degussa P25. Notably, the rGO/ TiO_2 composite shows obvious enhanced photocatalytic activity compared with TiO_2 ($W_R = 20.8\%$), indicating a significant synergistic effect of graphene for composite. It is found that the photocatalytic activity of the simply mixture of GO and TiO_2 sphere is also higher than that of TiO_2 hollow spheres and the commercial P25, while lower than the rGO/ TiO_2 composite. The enhancement of photocatalytic activity for rGO/ TiO_2 composite can be explained by the following factors. The TiO_2 with 20.8% rutile phase has synergistic effect between anatase and rutile, which favors the spatial separation of photo generated charge carriers, and offering a greater surface area for dye adsorption for dye binding. The as-obtained mixed phase TiO_2 plays a key role in preparing the rGO/ TiO_2 composite suggesting the importance of tuning the phase structure of TiO_2 . As we know, in 3D composite, the hollow spheres will be reasonable for the improvement of the photocatalytic activity.^{62,63} In the 3D rGO/ TiO_2 composite, the TiO_2 microspheres are wrapped in the reduced graphene sheets which can not only improve the electron conductivity of the material but prevent agglomeration or the irreversibly restack to form graphite. The crinkled texture of rGO and the close contact between catalyst particles and rGO sheets supply sufficient access for the catalytic reaction, thus ensuring that catalytic reaction can take place easily at the surface of the material, which is well consistent with the BET surface area. Moreover, the 3D structure buffers the

associated volume changes during the catalytic reaction as well. Therefore, it is reasonable that rGO/TiO₂ composite has a higher photocatalytic activity.

4 Conclusions

In summary, TiO₂ with controllable phase were successfully synthesized using solvothermal treatment by simply adjusting the amount/concentration of the surfactant. It is clearly demonstrated that the mixed phase TiO₂ with W_R is 20.8% show the highest photocatalytic activity. In order to further promote the photocatalytic performance, graphene-based TiO₂ composite was prepared with the aid of PLL and EG by a solvothermal route. TiO₂ particles were arranged on the rGO which via the solvothermal treatment. The photocatalytic property of as-prepared rGO/TiO₂ composite was also investigated in detail and it shows the enhanced photocatalytic activity compared to the simply mixture of TiO₂ and GO, original TiO₂, and the commercial P25 for the photocatalytic degradation of MB, because of the synergetic effects of mixed phase of TiO₂ between anatase and rutile, large surface area, novel structure, the utilization of rGO. This work provides a simple and effective strategy for the synthesis of high-performance TiO₂-based functional composite and it is of highly potential for photocatalytic use.

Acknowledgements

Financial supports from the National Natural Science Foundation of China (NSFC 21271053, 21001035, 51272050 and 51072038), Research Fund for the Doctoral Program of Higher Education of China (20112304110021), Natural Science Foundation of Heilongjiang Province (LC2012C10), Program for New Century Excellent Talents in University, Harbin Sci.-Tech. Innovation Foundation (RC2012XK017012), and the Fundamental Research Funds for the Central Universities of China are greatly acknowledged.

Notes and references

^a Key Laboratory of Superlight Materials and Surface Technology, Ministry of Education, College of Materials Science and Chemical Engineering, Harbin Engineering University, Harbin 150001, P. R. China. E-mail: yangpiaoping@hrbeu.edu.cn; gaopeng@hrbeu.edu.cn;

^b College of Science, Harbin Engineering University, Harbin, 150001, P. R. China. E-mail: chenyuujin@hrbeu.edu.cn

- M. Mrowetz, W. Balcerski, A. J. Colussi and M. R. Hoffmann, *J. Phys. Chem. B*, 2004, 108, 17269.
- M. R. Hoffmann, S. T. Martin, W. Choi and D. W. Bahnemann, *Chem. Rev.*, 1995, 95, 69.
- T. L. Thompson and J. T. Yates, *Top. Catal.*, 2005, 35, 197.
- R. Asahi, T. Morikawa, T. Ohwaki, K. Aoki and Y. Taga, *Science*, 2001, 293, 269.
- X. Chen and S. S. Mao, *Chem. Rev.*, 2007, 107, 2891.
- I. K. Konstantinou and T. A. Albanis, *Appl. Catal., B*, 2004, 49, 1.
- T. L. Thompson and J. T. Yates, *Chem. Rev.*, 2006, 106, 4428.
- F. E. Osterloh, *Chem. Mater.*, 2007, 20, 35.
- C. Sun, H. Li and L. Chen, *J. Phys. Chem. Solids*, 2007, 68, 1785.
- A. A. Ayon, M. Cantu, K. Chava, C. M. Agrawal, M. D. Feldman, D. Johnson, D. Patel, D. Marton and E. Shi, *Biomed. Mater.*, 2006, 1, 11.
- D. Wang, D. Choi, J. Li, Z. Yang, Z. Nie, R. Kou, D. Hu, C. Wang, L. V. Saraf, J. Zhang, I. A. Aksay and J. Liu, *ACS Nano*, 2009, 3, 907.
- J. L. Gole, J. D. Stout, C. Burda, Y. Lou and X. Chen, *J. Phys. Chem. B*, 2003, 108, 1230.
- F. Gao, Y. Wang, D. Shi, J. Zhang, M. Wang, X. Jing, R. Humphry Baker, P. Wang, S. M. Zakeeruddin and M. Graetzel, *J. Am. Chem. Soc.*, 2008, 130, 10720.
- T. Salthammer and F. Fuhrmann, *Environ. Sci. Technol.*, 2007, 41, 6573.
- Y. Zhang, P. He and N. Hu, *Electrochim. Acta*, 2004, 49, 1981.
- J. M. Macak, P. J. Barczuk, H. Tsuchiya, M. Z. Nowakowska, A. Ghicov, M. Chojak, S. Bauer, S. Virtanen, P. J. Kulesza and P. Schmuki, *Electrochem. Commun.*, 2005, 7, 1417.
- Y. Qiao, S. J. Bao, C. M. Li, X. Q. Cui, Z. S. Lu and J. Guo, *ACS Nano*, 2007, 2, 113.
- C. Y. Wang, R. Pagel, D. W. Bahnemann and J. K. Dohrmann, *J. Phys. Chem. B*, 2004, 108, 14082.
- S. J. Bao, C. M. Li, J. F. Zang, X. Q. Cui, Y. Qiao and J. Guo, *Adv. Funct. Mater.*, 2008, 18, 591.
- J. Zhang, Q. Xu, M. Li, Z. Feng and C. Li, *J. Phys. Chem. C*, 2009, 113, 1698.
- M. R. Hoffmann, S. T. Martin, W. Y. Choi and D. W. Bahnemann, *Chem. Rev.*, 1995, 95, 69.
- N. Wu, J. Wang, D. N. Tafen, H. Wang, J. G. Zheng, J. P. Lewis, X. Liu, S. S. Leonard and A. Manivannan, *J. Am. Chem. Soc.*, 2010, 132, 6679.
- J. Zhu, Z. Deng, F. Chen, J. Zhang, H. Chen, M. Anpo, J. Huang and L. Zhang, *Appl. Catal. B*, 2006, 62, 329.
- J. Yu, G. Wang, B. Cheng and M. Zhou, *Appl. Catal., B*, 2007, 69, 171.
- J. Zhang, Q. Xu, Z. Feng, M. Li and C. Li, *Angew. Chem. Int. Ed.*, 2008, 47, 1766.
- A. Biswas, A. Corani, A. Kathiravan, Y. Infahsaeng, A. Yartsev, V. Sundstrom and S. De, *Nanotechnology*, 2013, 24, 195601.
- J. Shi, J. Chen, Z. Feng, T. Chen, Y. Lian, X. Wang and C. Li, *J. Phys. Chem. C*, 2007, 111, 693.
- A. Testino, I. R. Bellobono, V. Buscaglia, C. Canevali, M. D'Arienzo, S. Polizzi, R. Scotti and F. Morazzoni, *J. Am. Chem. Soc.*, 2007, 129, 3564.
- G. Tian, H. Fu, L. Jing, B. Xin and K. Pan, *J. Phys. Chem. C*, 2008, 112, 3083.
- C. Kang, L. Jing, T. Guo, H. Cui, J. Zhou and H. Fu, *J. Phys. Chem. C*, 2008, 113, 1006.
- D. I. Enache, J. K. Edwards, P. Landon, B. Solsona-Espriu, A. F. Carley, A. A. Herzing, M. Watanabe, C. J. Kiely, D. W. Knight and G. J. Hutchings, *Science*, 2006, 311, 362.
- W. Zhao, W. Ma, C. Chen, J. Zhao and Z. Shuai, *J. Am. Chem. Soc.*, 2004, 126, 4782.
- T. Ohno, M. Akiyoshi, T. Umebayashi, K. Asai, T. Mitsui and M. Matsumura, *Appl. Catal. A*, 2004, 265, 115.
- V. Subramanian, E. E. Wolf and P. V. Kamat, *J. Am. Chem. Soc.*, 2004, 126, 4943.
- Z. Wen, S. Cui, H. Pu, S. Mao, K. Yu, X. Feng and J. Chen, *Adv. Mater.*, 2011, 23, 5445.
- T. H. Han, W. J. Lee, D. H. Lee, J. E. Kim, E. Y. Choi and S. O. Kim, *Adv. Mater.*, 2010, 22, 2060.
- Z. Wang, X. Zhou, J. Zhang, F. Boey and H. Zhang, *J. Phys. Chem. C*, 2009, 113, 14071.
- N. O. Weiss, H. Zhou, L. Liao, Y. Liu, S. Jiang, Y. Huang and X. Duan, *Adv. Mater.*, 2012, 24, 5782.
- N. N. Zhang, H. X. Qiu, Y. Liu, W. Wang, Y. Li, X. D. Wang and J. P. Gao, *J. Mater. Chem.*, 2011, 21, 11080.
- Z. S. Li, X. M. Huang, X. F. Zhang, L. Zhang and S. Lin, *J. Mater. Chem.*, 2012, 22, 23602.
- G. Lu, L. E. Ocola and J. Chen, *Nanotechnology*, 2009, 20, 445502.
- C. Nethravathi, T. Nisha, N. Ravishankar, C. Shivakumara and M. Rajamathi, *Carbon*, 2009, 47, 2054.
- C. Xu, X. Wang and J. Zhu, *J. Phys. Chem. C*, 2008, 112, 19841.
- C. Nethravathi and M. Rajamathi, *Carbon*, 2008, 46, 1994.
- X. Huang, Z. Zeng, Z. Fan, J. Liu and H. Zhang, *Adv. Mater.*, 2012, 24, 5979.
- Z. Wang, X. Zhou, J. Zhang, F. Boey and H. Zhang, *J. Phys. Chem. C*, 2009, 113, 14071.

- 47 X. Huang, Z. Y. Yin, S. X. Wu, X. Y. Qi, Q. Y. He, Q. C. Zhang, Q. Y. Yan, F. Boey and H. Zhang, *Small*, 2011, 7, 1876
- 48 H. Wang, H. S. Casalongue, Y. Liang and H. Dai, *J. Am. Chem. Soc.*, 2010, 132, 7472.
- 5 49 S. Guo, S. Dong and E. Wang, *ACS Nano*, 2009, 4, 547.
- 50 L. Qu, Y. Liu, J. B. Baek and L. Dai, *ACS Nano*, 2010, 4, 1321.
- 51 Y. Y. Liang, Y. G. Li, H. L. Wang, J. G. Zhou, J. Wang, T. Regier and H. J. Dai, *Nat. Mater.*, 2011, 10, 780.
- 52 Y. W. Zhu, S. Murali, M. D. Stoller, K. J. Ganesh, W. W. Cai, P. J. Ferreira, A. Pirkle, R. M. Wallace, K. A. Cychosz, M. Thommes, D. Su, E. A. Stach and R. S. Ruoff, *Science*, 2011, 332, 1537.
- 10 53 G. Zhou, D. W. Wang, F. Li, L. Zhang, N. Li, Z. S. Wu, L. Wen, G. Q. Lu and H. M. Cheng, *Chem. Mater.*, 2010, 22, 5306.
- 54 S. Chen, J. Zhu, X. Wu, Q. Han and X. Wang, *ACS Nano*, 2010, 4, 2822.
- 15 55 J. Zhang, Z. Zhu, Y. Tang and X. Feng, *J. Mater. Chem. A*, 2013, 1, 3752.
- 56 Y. Wang, S. L. Gai, N. Niu, F. He and P. P. Yang, *J. Mater. Chem. A*, 2013, 1, 9083.
- 20 57 Y. Wang, P. P. Yang, P. A. Ma, F. Y. Qu, S. L. Gai, N. Niu, F. He and J. Lin, *J. Mater. Chem. B*, 2013, 1, 2056.
- 58 Y. Wang, S. Gai, C. Li, F. He, M. Zhang, Y. Yan and P. Yang, *Electrochim. Acta.*, 2013, 90, 673.
- 59 J. Gao, F. Liu, Y. Liu, N. Ma, Z. Wang and X. Zhang, *Chem. Mater.*, 2010, 22, 2213.
- 25 60 Z. J. Fan, J. Yan, T. Wei, L. J. Zhi, G. Q. Ning, T. Y. Li and F. Wei, *Adv. Funct. Mater.*, 2011, 21, 2366.
- 61 J. W. Lee, A. S. Hall, J. D. Kim and T. E. Mallouk, *Chem. Mater.*, 2012, 24, 1158.
- 30 62 H. B. Zeng, G. T. Duan and Y. Li, *ACS Nano*, 2008, 2, 1661.
- 63 H. B. Zeng; P. S. Liu and W. P. Cai, *J. Phys. Chem. C.*, 2008, 112, 19620.